Available online at www.sciencedirect.com
SCIENCE DIRECT
Journal of Power Sources 154 (2006) 18–34
JOURNAL OF POWER SOURCES
www.elsevier.com/locate/jpowsour

Evaluation of the optimal separator shape with reaction and flow analysis of polymer electrolyte fuel cell

Gen Inoue *, Yosuke Matsukuma, Masaki Minemoto

Department of Chemical Engineering, Faculty of Engineering, Kyushu University, Hakozaki, Higashi-ku, Fukuoka 812-8581, Japan

Received 3 December 2004; received in revised form 4 March 2005; accepted 25 March 2005
Available online 15 June 2005

Abstract

The small polymer electrolyte fuel cell (PEFC) was experimented by changing operation temperature and H_2 and O_2 concentration in supply gas, and the PEFC reaction characteristic model that can express these influences was created. Moreover, PEFC reaction and flow analysis model was made with this reaction characteristic model and thermal flow analysis model. Furthermore, in order to improve the performance and the safety of PEFC, five kinds of separators were evaluated from the viewpoint of state of gas flow, uniformity of current density and temperature, reduction of pressure loss and exhaustibility of liquid water with this PEFC reaction and flow analysis model. In case of parallel separator, flow rate and current density distribution was not uniform, and exhaustibility of the liquid water was low. In case of serpentine separator, pressure drop was large. In addition, semi-serpentine separator was designed for the shape which combines parallel separator and serpentine separator, and the temperature and current density distribution of this separator was more uniform than any other separators, so this separator was excellent.

Keywords: PEFC; Numerical analysis; Current density distribution; Gas flow rate distribution; Separator

1. Introduction

At present, humankind have serious problems of environment, such as global warming and acid rain, and of lack of fuel sources, such as petroleum and natural gases. In order to contribute to the solution of these problems, fuel cell is expected to be practical use because it has low emission of environmental pollutant and high conversion efficiency from chemical energy to electrical energy. Especially, polymer electrolyte fuel cell (PEFC) is developed as power source of transportation and stationary family power supply in various fields, because it has low operation temperature and high power density. The materials development and the configuration design of separator, which is component of PEFC, are also researched.

In order to improve the power generation performance, the durability and the safety of PEFC, it is important to design the best separator shape to satisfy the following three conditions concerning the whole PEFC system: (1) the current density distribution and the gas flow rate distribution can be unified; (2) liquid water can be removed smoothly; (3) pressure drop of supply gas can be reduced. However, there are very few researches that examine the design of gas flow channel by considering internal phenomena while the electric power is generated. As the flow and mass transfer phenomena occur complicatedly between microscopic area and macroscopic area, it is very difficult to visualize and measure the phenomenon. Consequently, numerical analysis is useful to examine it. Bernardi and Verbrugge [1,2] and Springer et al. [3] developed one-dimensional model to the direction of membrane thickness, and examined concentration distribution and water management in PEFC. Fuller and Newman [4] analyzed and developed two-dimensional model to the direction of membrane thickness and gas flow channel. Nguyen and White [5], and Yi and Nguyen [6] developed heat and water transport models (2-D) that accounted for various operation conditions and membrane hydration

* Corresponding author. Tel.: +81 92 642 3523; fax: +81 92 642 3523.
E-mail address: ginoue@chem-eng.kyushu-u.ac.jp (G. Inoue).

0378-7753/$ – see front matter © 2005 Elsevier B.V. All rights reserved.
doi:10.1016/j.jpowsour.2005.03.216

Nomenclature

A_e	effective surface area per unit projection area of a electrode
A_s	effective surface area per unit amount of platinum ($m^2\,g^{-1}$)
b_c	condensation rate constant (s^{-1})
C_A	molar concentration of species A ($mol\,m^{-3}$)
C^e	molar concentration at interface between GDL and electrode ($mol\,m^{-3}$)
$C^f_{O_2}$	molar concentration of oxygen in electrolyte ($mol\,m^{-3}$)
$C^{f,ref}_{O_2}$	reference molar concentration of oxygen in electrolyte ($mol\,m^{-3}$)
C^g	molar concentration in the gas phase ($mol\,m^{-3}$)
$C^g_{O_2}$	molar concentration of oxygen in the gas phase ($mol\,m^{-3}$)
C_p	specific heat at constant pressure ($J\,kg^{-1}\,K^{-1}$)
$C^{(m)}_{H_2O}$	molar concentration at anode or cathode side interface of membrane ($mol\,m^{-3}$)
C_α	parameter used in the expression for cathodic transfer coefficient
C_σ	fitting parameter in Eq. (7)
D	diffusion coefficient ($m^2\,s^{-1}$)
D_A	diffusion coefficient of species A ($m^2\,s^{-1}$)
D_h	hydraulic diameter (m)
$D^m_{H_2O}$	effective diffusion of water in membrane ($m^2\,s^{-1}$)
E	electromotive force (V)
E^0	standard electromotive force (V)
$E_{\Delta H}$	the value of reduction change of water enthalpy to voltage (V)
f	effective porosity
F	Faraday's constant ($96{,}485\,C\,mol^{-1}$)
h	heat transfer coefficient ($J\,m^{-2}\,s^{-1}\,K^{-1}$)
ΔH_{H_2O}	change of water enthalpy between vapor and liquid ($J\,mol^{-1}$)
i	current density ($A\,cm^{-2}$)
i_0^+	exchange current density ($A\,cm^{-2}$)
i_0^{ref+}	exchange current density at reference O_2 concentration ($A\,cm^{-2}$)
i_L	limit current density ($A\,cm^{-2}$)
k	thermal conductivity ($J\,m^{-1}\,s^{-1}\,K^{-1}$)
k_{i_0}	proportionally constant of exchange current density
k_σ	fitting parameter in Eq. (7)
l^d	gas diffusion layer thickness (m)
l^g	gas channel depth (m)
l^s	thickness of solid phase (m)
L	inlet width (m)
m_{pt}	amount of platinum per unit electrode area ($g\,m^{-2}$)
M_j	molecular weight of species j ($kg\,mol^{-1}$)
M^m_{dry}	membrane dry equivalent weight
n	number of electrons participating in a reaction
n_d	electro-osmotic drag coefficient
p	pressure in Eq. (20) (Pa)
Δp	water ejection differential pressure in Eq. (35) (Pa)
P	pressure (Pa)
$P_{H_2O,sat}$	saturated vapor pressure in stream (Pa)
q_1	heat flux from MEA to gas phase ($J\,m^{-2}\,s^{-1}$)
q_2	heat flux from back plate to gas phase ($J\,m^{-2}\,s^{-1}$)
q_3	heat value generated by reaction per unit area ($J\,m^{-2}\,s^{-1}$)
q_4	heat flux from gas phase to solid phase ($J\,m^{-2}\,s^{-1}$)
q_5	heat flux from back plate to solid phase ($J\,m^{-2}\,s^{-1}$)
q_6	latent heat value of condensation per unit area ($J\,m^{-2}\,s^{-1}$)
r_j	molar flux of species j ($mol\,m^{-2}\,s^{-1}$)
R	gas constant ($8.314\,J\,mol^{-1}\,K^{-1}$)
t	time (s)
t_m	membrane thickness (m)
T	temperature (K)
T^b	cooling plate temperature (K)
T^g	gas phase temperature (K)
T^s	solid phase temperature (K)
$\boldsymbol{v}$	flow velocity vector ($m\,s^{-1}$)
v	flow velocity ($m\,s^{-1}$)
V	operation voltage (V)
x	horizontal distance (m)
Δx	distance on calculation mesh to neighboring gas channel (m)
y	horizontal distance (m)
z	vertical distance (m)

Greek letters

α	net water transfer coefficient
α^a	transfer coefficient in Eq. (5)
α^c_1	transfer coefficient in Eq. (6)
α^c_2	transfer coefficient in Eq. (11)
η_{act}	activation overvoltage (V)
η_{con}	concentration overvoltage (V)
η_{ohm}	ohmic resistance overvoltage (V)
λ	water content in the membrane
μ	viscosity of mixture (Pa s)
ρ	density of mixture ($kg\,m^{-3}$)
ρ^m_{dry}	membrane dry density ($kg\,m^{-3}$)
σ^m	membrane conductivity ($1\,\Omega^{-1}\,m^{-1}$)
σ^m_e	effective membrane conductivity ($1\,\Omega^{-1}\,m^{-1}$)
τ	viscous stress (Pa)
$\boldsymbol{\tau}$	viscous stress tensor (Pa)
ξ	activity water in stream

Superscripts

a	anode
b	back plate
c	cathode
g	gas phase
m	membrane
s	solid phase
sep	separator

Subscripts

A	species A
j	species *j*
H_2	hydrogen
H_2O(l)	liquid water
H_2O(v)	vapor water
MEA	membrane electrode assembly
N_2	nitrogen
O_2	oxygen

conditions. On the other hand, it is thought that analysis with the computational fluid dynamics (CFD) technique is important in order to calculate the transport phenomena in detail, and such study is increasing recently. Um et al. [7] and Wang et al. [8] have developed two-dimensional model with CFD, which included two-phase flow. Dutta et al. [9] made a three-dimensional computational model based on the commercial software package, *Fluent*. Berning et al. [10] presented a non-isothermal, three-dimensional models and calculated the distribution of current density and concentration in the straight channel. Mazumder and Cole [11] examined the liquid water transport with three-dimensional model. Li et al. [12] analyzed in small cell with three-dimensional analysis. Um and Wang [13] compared the performance of straight flow channel with that of interdigiteted flow channel by three-dimensional analysis. Kulikovsky [14] analyzed serpentine channel under the condition that gas inlet flow rate in each channel was constant. These PEFC numerical analysis models contributed to the optimization of component design and operation condition, and to the examination of issues included in present cell. However, these studies calculated internal phenomena in short straight gas channel and one serpentine channel or in small cell, and there are very few researches that evaluated various channel shapes of actual size cell under considering realistic calculation time and calculation resource.

In this study, the small PEFC was experimented with changing operation temperature, humidify temperature and H_2 and O_2 concentration in supply gas. The influence to the *i–V* characteristic was considered, and the PEFC reaction model that can express these influences was created. Next, the actual size PEFC reaction and flow analysis model was made with this reaction model and thermal flow analysis code. In addition, the water ejection condition was investigated by the one channel gas flow experiment. Finally, five kinds of separators were evaluated with this PEFC reaction and flow analysis model from the viewpoint of gas flow condition, current density distribution, cell temperature distribution, pressure drop, ejection performance of liquid water. And the best separator shape that can be safety and high performance was examined.

2. PEFC reaction model

2.1. Structure of small PEFC and experiment

Fig. 1 shows the structure of small PEFC in this experiment. Membrane electrode assembly (MEA), which is coated with Pt electrode on both sides of electrolyte membrane, is in the center of PEFC. MEA is sandwiched between two carbon gas diffusion layers (GDL) that improve repellency and gas diffusibility, and furthermore, this set is sandwiched between two separators that have a straight groove; a depth of gas flow groove is 1 mm, a width is 2 mm and a length is 50 mm. Anode gas (hydrogen as fuel) and cathode gas (oxygen as oxidant) flow in the each separator channel, respectively. Specification of MEA and GDL is shown in Table 1. Small cell was used because physical quantities, which are gas flow rate, concen-

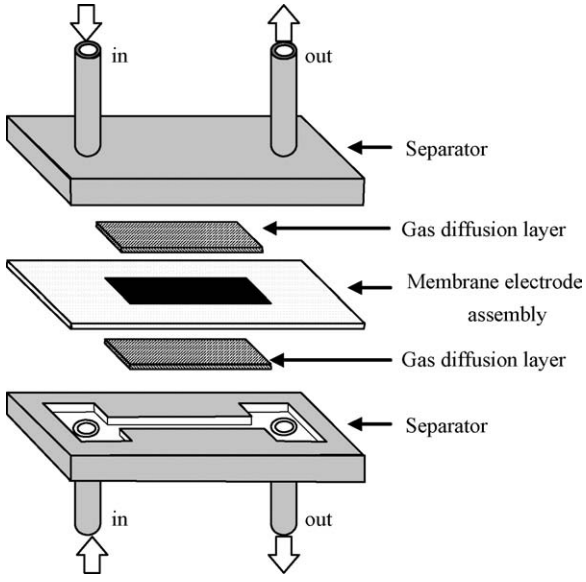

Fig. 1. Schematic diagram of small single cell.

Table 1
Specification of MEA and GDL of small cell

MEA	
Size of membrane (mm^2)	50×100
Thickness of membrane (μm)	30
Size of catalyst layer (mm^2)	10×50
Amount of Pt ($g\,m^{-2}$)	3.0
GDL	
Size (mm^2)	10×50
Thickness (μm)	300

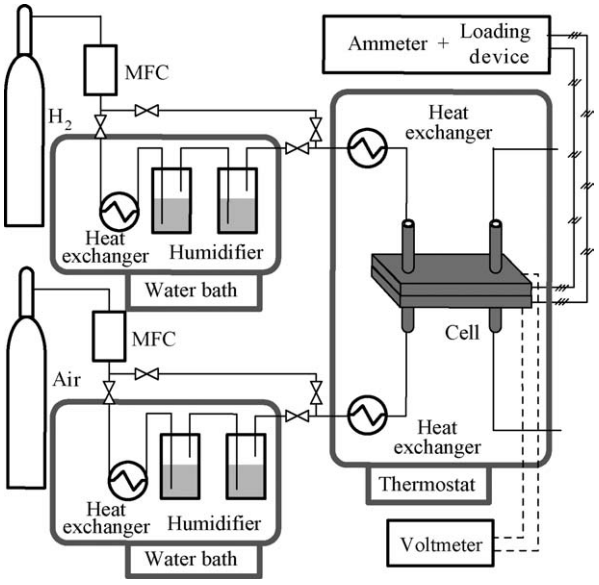

Fig. 2. Schematic diagram of experimental apparatus.

tration and temperature, have to be as uniform as possible in channel. Fig. 2 shows schematic of experimental apparatus. Anode gas was mixture gas of hydrogen and nitrogen, and hydrogen compositions were 3, 10, 30 and 100%. Cathode gas was mixture gas of oxygen and nitrogen, and oxygen compositions were 5, 10 and 21%. As electrolyte membrane is affected by moisture condition, humidification of supply gases is necessary in order to keep the water content and the ionic conductivity of membrane. Accordingly, external humidifier was set at the front of gas inlet of cell, and cell and humidifier were set in thermostat and water bath, respectively. The cell voltage and current were measured with multimeter and load. The operating condition is shown in Table 2. In order to decrease the concentration distribution due to cell reaction, hydrogen and oxygen utilizations were set to be less than 5%.

2.2. Assumptions of PEFC reaction model

Fig. 3 shows PEFC reaction simulation model. Operation voltage is calculated by following equation:

$$V = E - \eta^{a}_{act} - \eta^{c}_{act} - \eta^{a}_{con} - \eta^{c}_{con} - \eta^{m}_{ohm} \quad (1)$$

where V is operating voltage, E the electromotive force, η_{act} the activation overvoltage, η_{con} the concentration overvoltage, η_{ohm} the resistance overvoltage and the superscript a, c and m express anode, cathode and membrane, respectively. These overvoltage are caused by electrode reaction and transport phenomena at the parts shown in Fig. 3, respectively. In this study, the following parameters in these overvoltage model derived in the next section were used as fitting parameter to help the calculation data agree with experimental data in various conditions,

$$f^{a},\ f^{c},\ \alpha^{a},\ \alpha^{c}_{1},\ C_{\alpha},\ C_{\sigma}\ k_{\sigma},\ k_{i_0}$$

where f^{a} is the effective porosity of anode side GDL, f^{c} the effective porosity of cathode side GDL, α^{a} the transfer coefficient of anode concentration overvoltage, α^{c}_{1} the transfer coefficient of cathode concentration overvoltage, C_{α} the coefficient to calculate the transfer coefficient of activation overvoltage, C_{σ} and k_{σ} the correction coefficients to calculate the membrane ionic conductivity and k_{i_0} is the correction coefficients to calculate the exchange current density. Though there were some assumptions and models, which were not strict theoretically, the following models were developed in order only to use these value as fitting parameter.

Table 2
Operation conditions of small cell experiments

Cell temperature (K)	298, 313, 333, 363
Humidify temperature (K)	298, 313, 333, 363
O_2 composition (%)	5, 10, 21
H_2 composition (%)	3, 10, 30, 100
Pressure (MPa)	0.1
Anode gas flow rate ($m^3\ s^{-1}$)	3.33×10^{-6}
Cathode gas flow rate ($m^3\ s^{-1}$)	8.35×10^{-6}

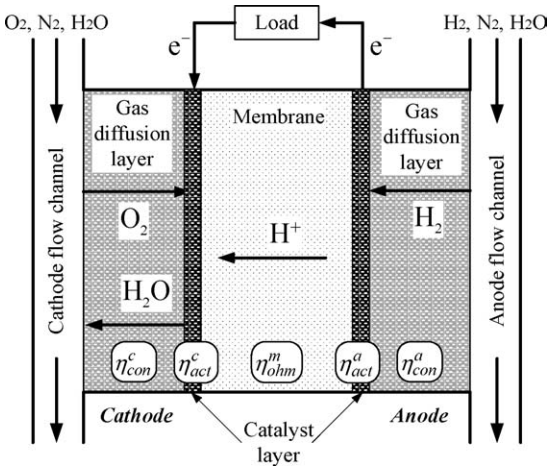

Fig. 3. PEFC reaction model.

These overvoltage equations are derived on the basis of the following assumption.

1. Gas concentration at the interface between gas flow channel and GDL is equal inlet gas concentration.
2. The reaction area reduction caused by flooding of electrode is ignored, and the diffusion prevention caused by water condensation is also ignored.
3. The heat of reaction is discharged out of PEFC, and the temperature of every PEFC component is constant.
4. In membrane, ionic conductivity, electro-osmosis coefficient and water effective diffusion coefficient that depend on membrane humidity are determined by water activity of anode side.
5. Anode activation overvoltage is ignored because it is lower than any other overvoltage.
6. The gas crossover is disregarded.

2.3. Derivations of PEFC reaction model

The electromotive force is shown by the following Nernst equation:

$$E = E^0 + \frac{RT}{nF} \ln \left[P^{\mathrm{a}}_{\mathrm{H_2}} \cdot (P^{\mathrm{c}}_{\mathrm{O_2}})^{1/2} \right] \tag{2}$$

where E^0 is standard electromotive force, R the gas constant, T the temperature, n the number of electrons participating in a reaction, F the Faraday's constant, $P^{\mathrm{a}}_{\mathrm{H_2}}$ the anode hydrogen partial pressure and $P^{\mathrm{c}}_{\mathrm{O_2}}$ is the cathode oxygen partial pressure.

Hydrogen that flows along the anode channel moves to interface of MEA and GDL through the GDL, and hydrogen concentration in the GDL decreases toward MEA. Consequently, assuming hydrogen concentration gradient is linear and constant in GDL with thickness l^{d}, current density can be calculated with $C^{\mathrm{g}}_{\mathrm{H_2}}$, which is concentration on interface of channel and GDL, and $C^{\mathrm{e}}_{\mathrm{H_2}}$, which is concentration on interface of GDL and MEA:

$$i = 2Ff^{\mathrm{a}} D_{\mathrm{H_2}} \frac{C^{\mathrm{g}}_{\mathrm{H_2}} - C^{\mathrm{e}}_{\mathrm{H_2}}}{l^{\mathrm{d}}} \tag{3}$$

where $D_{\mathrm{H_2}}$ is diffusion coefficient and f^{a} is the effective porosity of anode GDL. When $C^{\mathrm{e}}_{\mathrm{H_2}}$ is zero, concentration gradient and current density becomes maximum. The anode limiting current density is shown by the following equation. Similarly, cathode limiting current density can be calculated:

$$\begin{aligned} i_{\mathrm{L(H_2)}} &= 2Ff^{\mathrm{a}} D_{\mathrm{H_2}} \frac{C^{\mathrm{g}}_{\mathrm{H_2}}}{l^{\mathrm{d}}} = 2Ff^{\mathrm{a}} D_{\mathrm{H_2}} \frac{1}{l^{\mathrm{d}}} \frac{P^{\mathrm{g}}_{\mathrm{H_2}}}{RT} \\ i_{\mathrm{L(O_2)}} &= 4Ff^{\mathrm{c}} D_{\mathrm{O_2}} \frac{C^{\mathrm{g}}_{\mathrm{O_2}}}{l^{\mathrm{d}}} = 4Ff^{\mathrm{c}} D_{\mathrm{O_2}} \frac{1}{l^{\mathrm{d}}} \frac{P^{\mathrm{g}}_{\mathrm{O_2}}}{RT} \end{aligned} \tag{4}$$

Anode concentration overvoltage can be calculated by the following equation with the limiting current density:

$$\eta^{\mathrm{a}}_{\mathrm{con}} = -\frac{RT}{\alpha^{\mathrm{a}} 2F} \ln \left(1 - \frac{i}{i_{\mathrm{L(H_2)}}} \right) \tag{5}$$

Similarly, cathode concentration overvoltage can be calculated by the following equation:

$$\eta^{\mathrm{c}}_{\mathrm{con}} = -\frac{RT}{\alpha^{\mathrm{c}}_1 2F} \ln \left(1 - \frac{i}{i_{\mathrm{L(O_2)}}} \right) \tag{6}$$

where α^{a} and α^{c}_1 are transfer coefficient of anode and cathode, respectively.

The ionic conductivity of electrolyte membrane is calculated by the Springer et al. method [3]. In this study, in order to agree with experimental and calculation data, the following modified the equation of Springer et al. is used:

$$\sigma^{\mathrm{m}}_{\mathrm{e}} = (0.514 C_\sigma \lambda - 0.326 k_\sigma) \times \exp \left[1268 \left(\frac{1}{303} - \frac{1}{T} \right) \right] \tag{7}$$

where C_σ and k_σ are constant. C_σ and k_σ were equal to 1 in the equation of Springer et al. However, as the membrane that was used in Springer's experiment was different from one of this experiment, so the ionic conductivity of this study is calculated with these parameter that were fitting parameter satisfied the coincidence with experimental and calculation results. Nguyen and White [5] applied water content of anode side to water content in Eq. (7). Water content of anode side is calculated with the anode water activity.

$$\begin{aligned} \lambda^{\mathrm{a}} &= 0.043 + 17.8\xi^{\mathrm{a}} - 39.8(\xi^{\mathrm{a}})^2 + 36.0(\xi^{\mathrm{a}})^3 \quad (\xi^{\mathrm{a}} \le 1) \\ \lambda^{\mathrm{a}} &= 14 + 1.4(\xi^{\mathrm{a}} - 1) \quad (\xi^{\mathrm{a}} > 1) \end{aligned} \tag{8}$$

Anode water activity is shown by the following equation:

$$\xi^{\mathrm{a}} = \frac{P^{\mathrm{a}}_{\mathrm{H_2O}}}{P^{\mathrm{a}}_{\mathrm{H_2O,sat}}} \tag{9}$$

Saturated vapor pressure is calculated by Antoine equation. Resistance overvoltage is shown by the following equation:

$$\eta_{\mathrm{ohm}} = \frac{t^{\mathrm{m}}}{\sigma^{\mathrm{m}}_{\mathrm{e}}} i \tag{10}$$

where t^{m} is thickness of membrane.

Anode activation overvoltage is calculated by the following Tafel equation:

$$\eta_{\mathrm{act}} = \frac{RT}{\alpha^{\mathrm{c}}_2 F} \ln \frac{i}{A_{\mathrm{e}} i^+_0} \tag{11}$$

where A_{e} is effective surface area per unit projection area of electrode.

$$A_{\mathrm{e}} = m_{\mathrm{pt}} A_{\mathrm{S}} \tag{12}$$

where m_{pt} is the amount of platinum per unit electrode area and A_{S} is effective surface area per unit amount of platinum. A_{S} is obtained in the effective surface area data of Marr and Li [15]. i^+_0 is oxygen exchange current density, and it is obtained by the following equation in reference [16]:

$$i^+_0 = i^{\mathrm{ref}+}_0 \left(\frac{C^{\mathrm{f}}_{\mathrm{O_2}}}{C^{\mathrm{f,ref}}_{\mathrm{O_2}}} \right) \tag{13}$$

$$C^{\mathrm{f,ref}}_{\mathrm{O_2}} = \frac{P^{\mathrm{c}}_{\mathrm{O_2}}}{\exp(14.1 - 666/T)} \tag{14}$$

$$C^{\mathrm{f}}_{\mathrm{O_2}} = 0.07 C^{\mathrm{g}}_{\mathrm{O_2}} \tag{15}$$

where $C^{\mathrm{f,ref}}_{\mathrm{O_2}}$ is the reference oxygen molar concentration in the electrolyte, $C^{\mathrm{f}}_{\mathrm{O_2}}$ the oxygen molar concentration in the electrolyte and $C^{\mathrm{g}}_{\mathrm{O_2}}$ is the molar concentration of oxygen in

the catalyst layer. In this study, it is assumed that $C^{g}_{O_2}$ is equal the concentration in gas flow channel. i_0^{ref} is exchange current density at reference oxygen concentration, and it is calculated by the following equation which is obtained by Parthasarathy et al. [17]:

$$\log_{10}(i_0^{ref+}) = 3.507 - \frac{4001}{T} \tag{16}$$

The MEA that was used in Parthasarathy's experiment was different from one of this experiment, so the exchange current density at reference oxygen concentration of this study is calculated by the following equation:

$$i_{0,e}^{ref+} = k_{i_0} i_0^{ref+} \tag{17}$$

where k_{i_0} is constant. α_2^c of Eq. (11) is calculated by the following equation [10]:

$$\alpha_2^c = C_\alpha + 2.3 \times 10^{-3}(T - 303.15) \tag{18}$$

Local current density is obtained with the above equations. But, in case current density is smaller than $A_e i_0^+$, activation overvoltage becomes negative. Therefore, it has to be taken that this model is not applicable on such current density condition.

In this study, the result and method of Parthasarathy et al. and Yoshikawa et al. were used in order to calculate the activation overvoltage. However, this combination is inappropriate theoretically because these result and equation were obtained in different experimental conditions from each other. That is why we corrected this model by fitting several parameters with experimental data and reduced the influence of the gap between different experimental conditions. As the current density–voltage curve shown in Figs. 8–11, it is possible to confirm that the influence of that gap were low.

3. PEFC thermal flow model

3.1. Structure of analytical model and assumption

Fig. 4 shows the structure of PEFC thermal flow model. Gas flow, concentration and temperature are calculated in the gas flow channel of anode and cathode. Assuming temperature of membrane, electrode and GDL are equal to each other, current density and temperature are calculated with the combination of these three components above. The combination of them is expressed to be solid phase. The governing equations are derived on the basis of the following assumption:

1. The volume of the condensation water is ignored, and the water moves with the gas.
2. The reaction area reduction caused by flooding of electrode is ignored, and the diffusion prevention caused by water condensation is also ignored.
3. Fluid is incompressible Newtonian fluid and ideal gas. Flow condition is laminar flow.

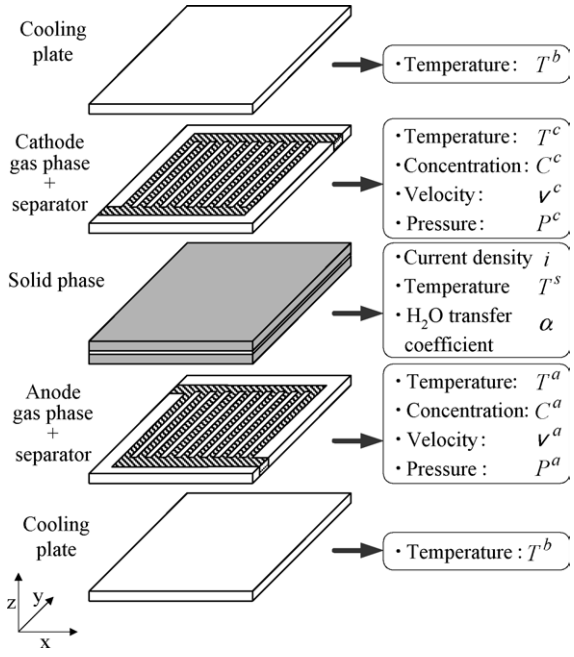

Fig. 4. Schematic diagram of PEFC reaction and flow analysis model.

4. Heat transfer between separator and gas is ignored. But heat transfer among gas phase, solid phase and back plate is calculated. Back plate temperature is constant.
5. Cell voltage is uniform and constant.
6. Cooling plates are inserted between every three cells, and the length of heat conduction between cooling plate and solid phase is lengthened three times as long as the thickness of single cell.
7. The flux of water through membrane is constant between both interface of anode side and cathode side.

3.2. Derivations of governing equation of PEFC flow analysis model

The direction of membrane surface is two-dimension (x–y), and the two-dimensional governing equations were derived. The continuity equation of anode and cathode gas is shown by the following equation:

$$(\nabla \cdot \boldsymbol{v}) = -\frac{1}{l^g \rho}\left[\sum_j M_j r j\right] \tag{19}$$

where $\boldsymbol{v}$ is the velocity vector of mixture gas, l^g the depth of gas channel, ρ the density of mixture gas, M_j the molecular weight of chemical species j and r_j is the reaction or condensation rate per unit area of chemical species j.

The equation of motion is shown by the following expression:

$$\rho\frac{D\boldsymbol{v}}{Dt} = -\nabla p - [\nabla \cdot \boldsymbol{\tau}] - \rho\boldsymbol{v}(\nabla \cdot \boldsymbol{v}) \tag{20}$$

where p is pressure and the operator D/Dt is substantial time derivative, $\boldsymbol{\tau}$ is viscous stress tensor that is shown by the

following expression:

$$\tau_{xx} = -2\mu\frac{\partial v_x}{\partial x} + \frac{2}{3}\mu(\nabla\cdot\boldsymbol{v}), \qquad \tau_{xy} = -\mu\left(\frac{\partial v_x}{\partial y} + \frac{\partial v_y}{\partial x}\right),$$
$$\tau_{yy} = -2\mu\frac{\partial v_y}{\partial y} + \frac{2}{3}\mu(\nabla\cdot\boldsymbol{v}) \tag{21}$$

where μ is the viscosity of mixture gas. And in order to include the effect of viscous drag from both walls that are GDL and the bottom of channel, Hele–Shaw model shown following was used:

$$\frac{\partial\tau_{zx}}{\partial z} = \frac{12\mu v_x}{(l^{\mathrm{g}})^2}, \qquad \frac{\partial\tau_{zy}}{\partial z} = \frac{12\mu v_y}{(l^{\mathrm{g}})^2} \tag{22}$$

The equation of mass balance of chemical species A is shown by the following equation:

$$\frac{\mathrm{D}C_{\mathrm{A}}}{\mathrm{D}t} = D_{\mathrm{A}}\nabla^2 C_{\mathrm{A}} - \frac{r_{\mathrm{A}}}{l^{\mathrm{g}}} - C_{\mathrm{A}}(\nabla\cdot\boldsymbol{v}) \tag{23}$$

where C_{A} is the concentration of chemical species A and D_{A} is the diffusion coefficient. The equations of mass balance were derived to eight kinds of $C^{\mathrm{a}}_{\mathrm{H_2}}$, $C^{\mathrm{a}}_{\mathrm{N_2}}$, $C^{\mathrm{a}}_{\mathrm{H_2O(v)}}$, $C^{\mathrm{a}}_{\mathrm{H_2O(l)}}$, $C^{\mathrm{c}}_{\mathrm{O_2}}$, $C^{\mathrm{c}}_{\mathrm{N_2}}$, $C^{\mathrm{c}}_{\mathrm{H_2O(v)}}$, $C^{\mathrm{c}}_{\mathrm{H_2O(l)}}$ that are hydrogen, oxygen, nitrogen, vapor and condensed water in anode and cathode channel.

The equation of mass balance of condensed water is shown by the following equation:

$$\frac{\mathrm{D}C_{\mathrm{H_2O(l)}}}{\mathrm{D}t} = -\frac{r_{\mathrm{H_2O(l)}}}{l^{\mathrm{g}}} - C_{\mathrm{H_2O(l)}}(\nabla\cdot\boldsymbol{v}) \tag{24}$$

The equation of energy of anode and cathode gas is shown by the following equation:

$$\rho^{\mathrm{g}}C^{\mathrm{g}}_{\mathrm{p}}\frac{\mathrm{D}T^{\mathrm{g}}}{\mathrm{D}t} = k^{\mathrm{g}}\nabla^2 T^{\mathrm{g}} + \frac{1}{l^{\mathrm{g}}}(q_1+q_2) - \rho^{\mathrm{g}}C^{\mathrm{g}}_{\mathrm{p}}T^{\mathrm{g}}(\nabla\cdot\boldsymbol{v}) \tag{25}$$

where C_{p} is the specific heat, T the temperature, k the thermal conductivity, the superscript g expresses anode gas or cathode gas, q_1 and q_2 are heat flux from solid phase and cooling plate, respectively,

$$q_1 = h(T^{\mathrm{s}} - T^{\mathrm{g}}), \qquad q_2 = h(T^{\mathrm{b}} - T^{\mathrm{g}}) \tag{26}$$

where h is heat transfer coefficient, T^{s} the temperature of solid phase and T^{b} is the temperature of cooling plate.

The equation of energy of solid phase is shown by the following equation:

$$\rho^{\mathrm{s}}C^{\mathrm{s}}_{\mathrm{p}}\frac{\partial T^{\mathrm{s}}}{\partial t} = k^{\mathrm{s}}\nabla^2 T^{\mathrm{s}} + \frac{1}{l^{\mathrm{s}}}(q_3+q_4+q_5+q_6) \tag{27}$$

where l^{s} is the thickness of solid phase, the superscript s expresses solid phase. q_3 is the heating value owing to electrochemical reaction per unit area and time, q_4 the heat flux from gas, q_5 the heat flux from cooling plate and q_6 is the latent heating value of condensation per unit area and time. These heat flux and heating value are shown by the following equation:

$$\begin{aligned}
q_3 &= (E_{\Delta H} - V)i \\
q_4 &= h^{\mathrm{a}}(T^{\mathrm{a}} - T^{\mathrm{s}}) + h^{\mathrm{c}}(T^{\mathrm{c}} - T^{\mathrm{s}}) \\
q_5 &= k^{\mathrm{sep}}\frac{T^{\mathrm{b}} - T^{\mathrm{s}}}{l^{\mathrm{g}}} \\
q_6 &= l^{\mathrm{g}}\,\Delta H_{\mathrm{H_2O}} b_{\mathrm{c}}\left(C^{\mathrm{a}}_{\mathrm{H_2O(v)}} - \frac{P^{\mathrm{a}}_{\mathrm{H_2O,sat}}}{RT^{\mathrm{a}}}\right) \\
&\quad + l^{\mathrm{g}}\,\Delta H_{\mathrm{H_2O}} b_{\mathrm{c}}\left(C^{\mathrm{c}}_{\mathrm{H_2O(v)}} - \frac{P^{\mathrm{c}}_{\mathrm{H_2O,sat}}}{RT^{\mathrm{c}}}\right)
\end{aligned} \tag{28}$$

where $E_{\Delta H}$ is the value of reduction change of water enthalpy to voltage, k^{sep} the heat conductivity of separator, $\Delta H_{\mathrm{H_2O}}$ the change of water enthalpy between vapor and liquid and b_{c} is the condensation rate constant.

The reaction and condensation rates of each ingredient are shown by the following equation:

$$\begin{aligned}
r^{\mathrm{a}}_{\mathrm{H_2}} &= \frac{i}{2F} \\
r^{\mathrm{a}}_{\mathrm{H_2O(v)}} &= \alpha\frac{i}{F} + l^{\mathrm{g}}b_{\mathrm{c}}\left(C^{\mathrm{a}}_{\mathrm{H_2O(v)}} - \frac{P^{\mathrm{a}}_{\mathrm{H_2O,sat}}}{RT^{\mathrm{a}}}\right) \\
r^{\mathrm{a}}_{\mathrm{N_2}} &= 0 \\
r^{\mathrm{a}}_{\mathrm{H_2O(l)}} &= -l^{\mathrm{g}}b_{\mathrm{c}}\left(C^{\mathrm{a}}_{\mathrm{H_2O(v)}} - \frac{P^{\mathrm{a}}_{\mathrm{H_2O,sat}}}{RT^{\mathrm{a}}}\right) \\
r^{\mathrm{c}}_{\mathrm{O_2}} &= \frac{i}{4F} \\
r^{\mathrm{c}}_{\mathrm{H_2O(v)}} &= -(1+2\alpha)\frac{i}{2F} + l^{\mathrm{g}}b_{\mathrm{c}}\left(C^{\mathrm{c}}_{\mathrm{H_2O(v)}} - \frac{P^{\mathrm{c}}_{\mathrm{H_2O,sat}}}{RT^{\mathrm{c}}}\right) \\
r^{\mathrm{c}}_{\mathrm{N_2}} &= 0 \\
r^{\mathrm{c}}_{\mathrm{H_2O(l)}} &= -l^{\mathrm{g}}b_{\mathrm{c}}\left(C^{\mathrm{c}}_{\mathrm{H_2O(v)}} - \frac{P^{\mathrm{c}}_{\mathrm{H_2O,sat}}}{RT^{\mathrm{c}}}\right)
\end{aligned} \tag{29}$$

where α is water transfer coefficient.

Current density is calculated by the above PEFC reaction model, which is shown in Eqs. (1)–(18), and that model is shown by the following equation with local concentration, the temperature and saturated vapor pressure:

$$i = f(V, C^{\mathrm{a}}_{\mathrm{H_2}}, C^{\mathrm{a}}_{\mathrm{H_2O(v)}}, C^{\mathrm{c}}_{\mathrm{O_2}}, T^{\mathrm{s}}, P^{\mathrm{a}}_{\mathrm{H_2O,sat}}) \tag{30}$$

It is assumed that water moves by electro-osmosis effect and back diffusion effect in electrolyte membrane. Water transfer coefficient expresses the number of net moving water molecules from anode to cathode through the membrane, when one proton transfers through the membrane. And it is calculated by the following equation shown by Nguyen and White [5]:

$$\alpha = n_{\mathrm{d}} - \frac{F}{i}D^{\mathrm{m}}_{\mathrm{H_2O}}\frac{C^{\mathrm{c(m)}}_{\mathrm{H_2O}} - C^{\mathrm{a(m)}}_{\mathrm{H_2O}}}{t_{\mathrm{m}}} \tag{31}$$

where n_d is the electro-osmotic drag coefficient, $D^m_{H_2O}$ the effective diffusion of water in membrane, $C^{c(m)}_{H_2O}$ the molar concentration at cathode side interface of membrane, $C^{a(m)}_{H_2O}$ the molar concentration at anode side interface of membrane and t_m is the membrane thickness. n_d and $D^m_{H_2O}$ are obtained by the following equations:

$$n_d = 0.0049 + 2.02\xi^a - 4.53(\xi^a)^2 + 4.09(\xi^a)^3 \quad (\xi^a \le 1)$$
$$n_d = 1.59 + 0.159(\xi^a - 1) \quad (\xi^a > 1) \tag{32}$$

$$D^m_{H_2O} = \left[0.0049 + 2.02\xi^a - 4.53(\xi^a)^2 + 4.09(\xi^a)^3\right] D^0 \times \exp\left[2416\left(\frac{1}{303} - \frac{1}{T^s}\right)\right] \quad (\xi^a \le 1)$$
$$D^m_{H_2O} = \left[1.59 + 0.159(\xi^a - 1)\right] D^0 \times \exp\left[2416\left(\frac{1}{303} - \frac{1}{T^s}\right)\right] \quad (\xi^a > 1) \tag{33}$$

where D^0 is effective diffusion of water in membrane at standard condition. $C^{a(m)}_{H_2O}$ and $C^{c(m)}_{H_2O}$ are shown by the following equations:

$$C^{k(m)}_{H_2O} = \frac{\rho^m_{dry}}{M^m_{dry}}\left[0.043 + 17.8\xi^k - 39.8(\xi^k)^2 + 36.0(\xi^k)^3\right] \quad (\xi^k \le 1)$$
$$C^{k(m)}_{H_2O} = \frac{\rho^m_{dry}}{M^m_{dry}}\left[14 + 1.4(\xi^k - 1)\right] \quad (\xi^k > 1) \tag{34}$$

where ρ^m_{dry} is the membrane dry density and M^m_{dry} is the membrane dry equivalent weight.

Eqs. (1)–(34) are connected in their respective group, such as reaction, concentration, temperature and flow and their partial differential equations are discretized by finite differential method. The boundary conditions of flow velocity, temperature and concentration are set as followings:

(1) *Gas inlet boundary*: these variables are constant.
(2) *Gas outlet boundary*: the gradients of these variables are constant.
(3) *Wall boundary*: the gradients of temperature and concentration are constant, and flow velocity is zero.

Current density and water transfer coefficient were calculated all over the electrode area. In case of calculation of these variables at gas channel area, the local concentration and temperature at that point were used as the needed variables. In case of calculation of these variables at no gas channel area (at shoulder area), the local values at adjoining gas channel were used. In this case, the diffusion length, l^d, was changed to $\sqrt{(l^d)^2 + (\Delta x)^2}$ in Eq. (4) that calculates the limiting current density, and gas diffusibility to shoulder area was considered. Δx is the distance on calculation mesh to adjoining gas channel. And the reaction rate of this shoulder area was put in the balance equations of adjoining mesh point at gas channel, and the conservation low was satisfied in single cell. Table 3 shows the calculation system and method used in this study and Fig. 5 shows calculation flow chart. Eqs. (1)–(34) were calculated until all variables became constant.

Table 3
Calculation system and method used in this study

Analysis dimension	2-D
Coordinate system	Rectangular coordinates
Digitization of space	Finite difference method
Handing of convection term	QUICKER method
Making time dispersed	Adams–Bashforth scheme
Flow analysis algorithm	FS method
Iteration of pressure	SOR method
Mesh	Square staggered mesh, 480 × 480

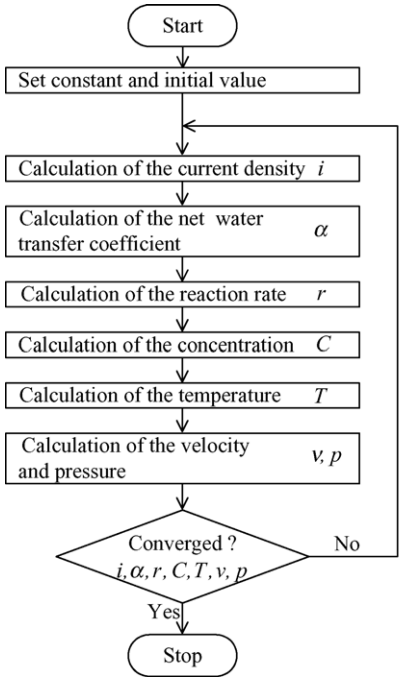

Fig. 5. Solution scheme for PEFC analysis.

4. Water ejection experiment

As PEFC is driven under 100 °C, supplied or generated water may be condensed and become liquid, and moreover, gas flow may be inhibited by the condensed water. And it is thought that this problem results in the cell instability, the decrease of cell output and the decline of durability. In this study, water ejection condition was obtained by the experiment on the assumption that condensed water block the channel. Fig. 6 shows the experimental apparatus. U shape pipe was connected to the one side of the channel blocked by the water, and length of the blocking water was between 10 and 20 mm. Water drop was dripped to the U shape pipe, and it pressurized the one side of blocking water, and the differential pressure that was able to eject water was measured. (This differential pressure is expressed as the ejection

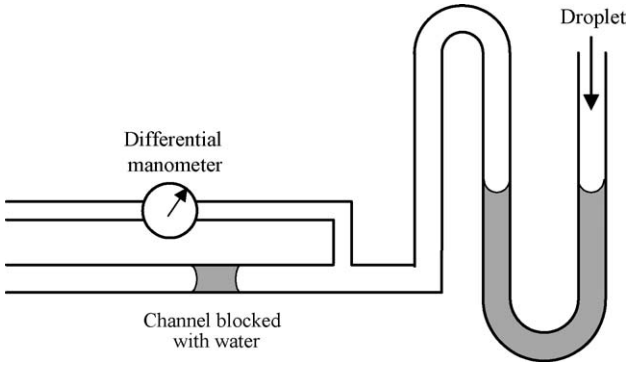

Fig. 6. Schematic diagram of liquid water ejection experimental apparatus.

differential pressure.) Three kinds of tube, which are circular tube made of halocarbon resin (A), rectangle tube made of acrylic resin (B) and circular glass tube (C), were used in this experiment. As a result, it turned out that the ejection differential pressure was not affected by the blocking water size, shape or material of the tube, but by only tube diameter. Fig. 7 shows the relationship between diameter and ejection differential pressure. Diameter of rectangular tube was calculated as hydraulic diameter. Fig. 7 means that as the hydraulic diameter decreases, the ejection differential pressure rises. The following ejection differential pressure equation was obtained in Fig. 7:

$$\Delta P = 1.04 \times 10^{-2} D_{\mathrm{h}}{}^{-1.42} \tag{35}$$

where Δp is the ejection differential pressure and D_{h} is the hydraulic diameter.

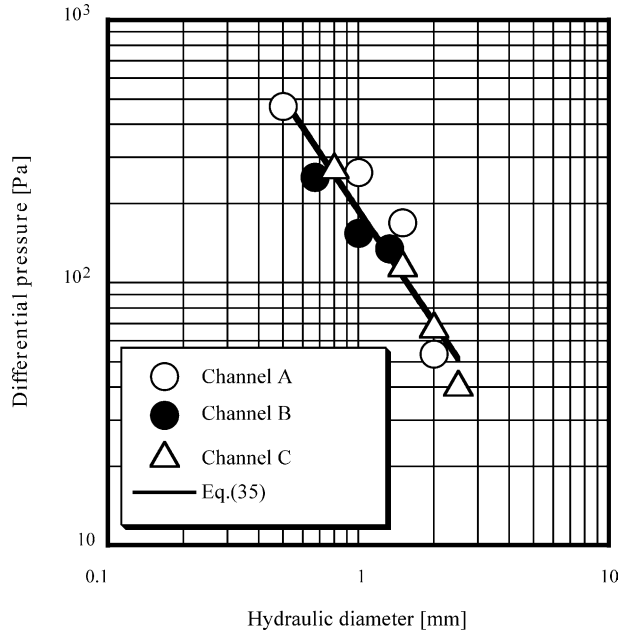

Fig. 7. Relationship between the hydraulic diameter and ejection differential pressure.

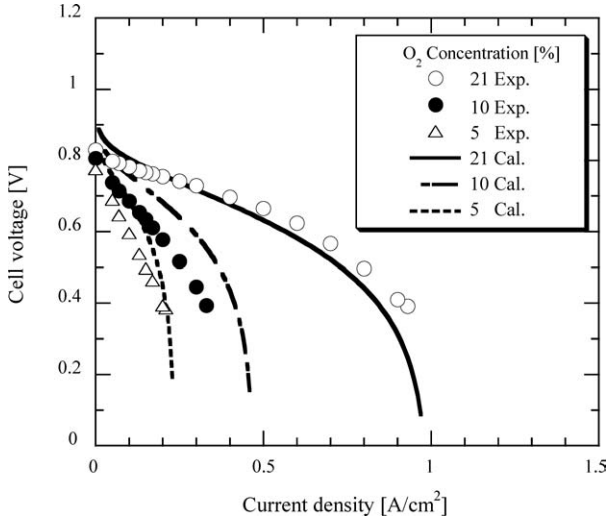

Fig. 8. Effect of O_2 concentration on cell voltage/current density plots with experimental and calculated results; cell temperature is 333 K, humidify temperature is 333 K and hydrogen composition is 100%.

5. Results and discussions

5.1. Experimental and calculation results of PEFC reaction model

In order to construct the PEFC reaction model, the effect of changing operation temperature, humidify temperature and hydrogen and oxygen concentration in supply gas on the current density and voltage characteristic of a small PEFC was examined experimentally. And the parameters (f^{a}, f^{c}, α^{a}, α_1^{c}, C_α, C_σ k_σ, k_{i_0}) that are applicable on all operation condition were decided by trial and error method with experimental results and Eqs. (1)–(18). The decided values of these parameters are shown in Table 4. The diffusion coefficient of hydro-

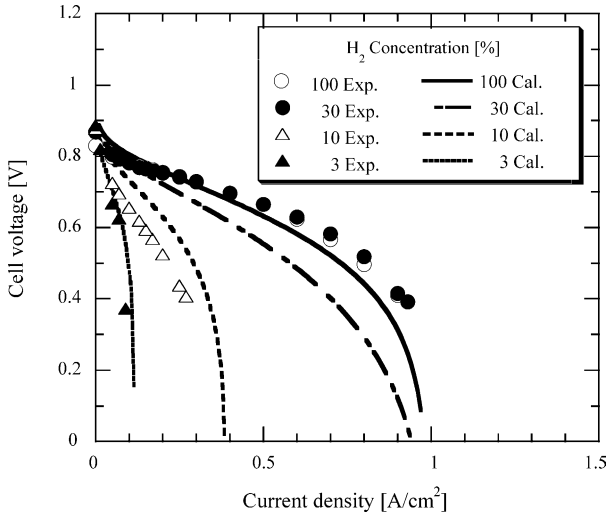

Fig. 9. Effect of H_2 concentration on cell voltage/current density plots with experimental and calculated results; cell temperature is 333 K, humidify temperature is 333 K and oxygen composition is 21%.

Table 4
Fitting parameters decided by experiments with small cell

$f^a = 0.020$
$f^c = 0.043$
$\alpha^a = 0.10$
$\alpha_1^c = 0.09$
$C_\alpha = 0.98$
$C_\sigma = 2.0$
$k_\sigma = 0.15$
$k_{i_0} = 1.0$

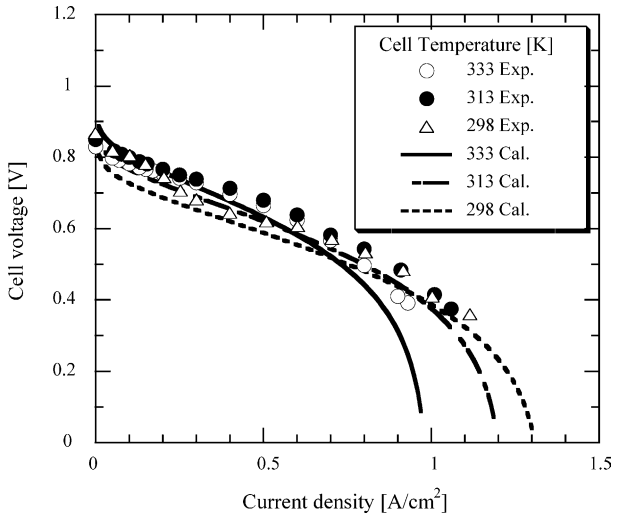

Fig. 10. Effect of cell temperature on cell voltage/current density plots with experimental and calculated results; humidify temperature is equal to cell temperature, hydrogen composition is 100% and oxygen composition is 21%.

gen and oxygen were 1.03×10^{-4} and $2.91 \times 10^{-5}\ m^2\ s^{-1}$, respectively, and the standard electromotive force was 1.23 V. Figs. 8 and 9 show experimental data and calculation data in case of changing oxygen and hydrogen concentration in supply gas, respectively. From these graphs, as oxygen and hydrogen concentration in supply gas were lower, the cell voltage reduced by concentration overvoltage. Fig. 10 shows the results in case of changing cell and the humidifier temperature. The humidify temperature was equal to the cell temperature. In case the cell temperature and the humidify temperature were high, the cell voltage was high in low current density because the activation overvoltage reduced, but the cell voltage was low in high current density because of the following cause. When the humidify temperature was high, water vapor concentration of supply gas increased, and oxygen concentration of supply gas decreased relatively. And the oxygen concentration overvoltage reduced the cell voltage. Fig. 11 shows the result of changing the humidifier temperature. The cell temperature was constant. As the humidify temperature were lower, the cell voltage reduced because of low ionic conductivity of membrane. In these graphs, the calculation results mostly agree with the experimental results.

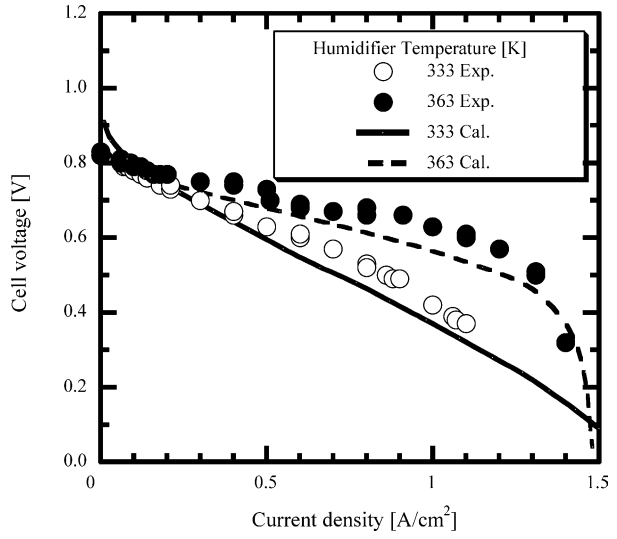

Fig. 11. Effect of humidification temperature on cell voltage/current density plots with experimental and calculated results; cell temperature is 363 K, hydrogen composition is 100% and oxygen composition is 21%.

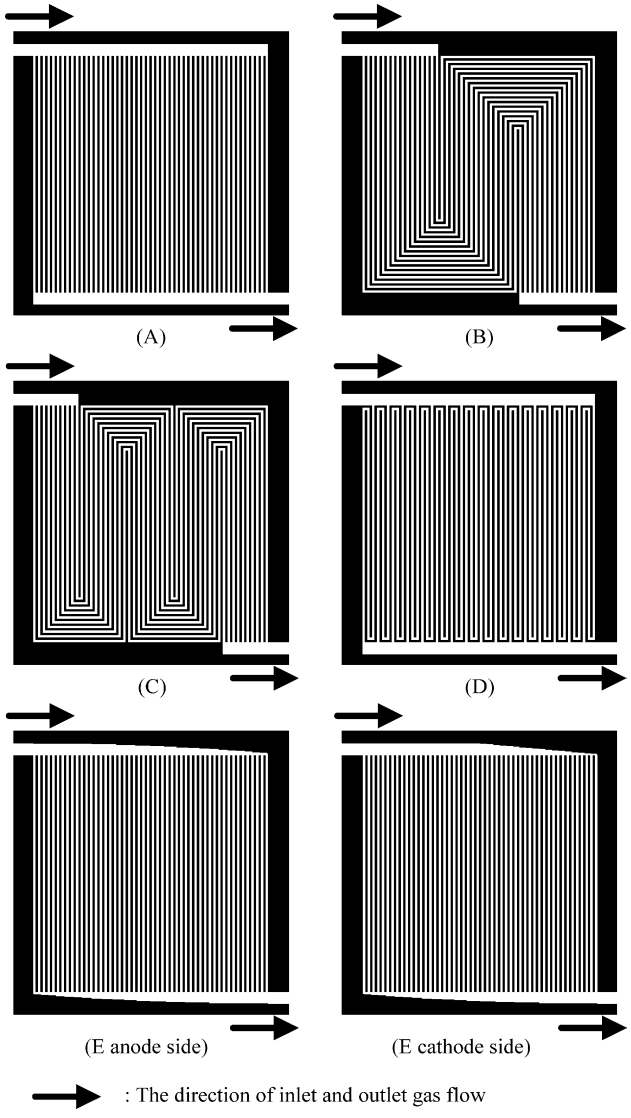

Fig. 12. (A–E) Shapes of five kinds of PEFC separators.

But hydrogen concentration overvoltage is discussed in here. In this experiment, anode GDL and cathode GDL were equal, and it is thought that anode effective porosity, f^a, and cathode effective porosity, f^c, must be the same essentially. Moreover, in case that flooding by cathode generation water strongly affects oxygen diffusion, it is thought that f^a must be larger than f^c. But the repellency of the surface of anode gas channel and GDL may have dropped in this experiment, and so the blocking of the hydrogen diffusion may have occurred. On the other hand, it is guessed that there were the gap between Fick's diffusion model and actual diffusion condition, and that hydrogen diffusion coefficient in calculation was excessive value. The gap of calculation and experimental results by changing hydrogen concentration in Fig. 9 was larger than that by changing other condition (Figs. 8, 10 and 11). Accordingly, it seems that the accuracy of f^a is lower than that of other parameter. The next section deals with the calculation results in detail, and it explains that average hydrogen concentration overvoltage was about 1% of the whole overvoltage, and hydrogen mass transfer in GDL did not affect the whole cell system. So, it is able to say that this problem about the accuracy of anode effective porosity f^a did not affect the calculation result very much. However, it is thought that the anode concentration overvoltage with high accuracy will be needed in case of other operating condition. In the future, the accuracy of this model will need to be increased by similar experiments. Concerning other parameter, the PEFC reaction model that can estimate current density and voltage characteristic on various operation conditions was constructed with the parameters of Table 4.

5.2. Results of PEFC reaction and flow analysis in five kinds of separator

Fig. 12 shows five kinds of separator shape that is object of this study. The electrode area was a 100 mm square. The width of the gas inlet and outlet header was 5 mm, and the depth was 1 mm. These separators were the parallel separator A that all channels were straight, serpentine separator B that all channels were bunched and they turned twice, serpentine separator C that all channels were bunched and they turned four times, semi-serpentine separator D that was designed as the shape to combine the parallel separator with the serpentine separator, and the parallel separator E that was partially improved shape of separator A in order to make gas flow rate distribution uniform. In the concrete, separator E was

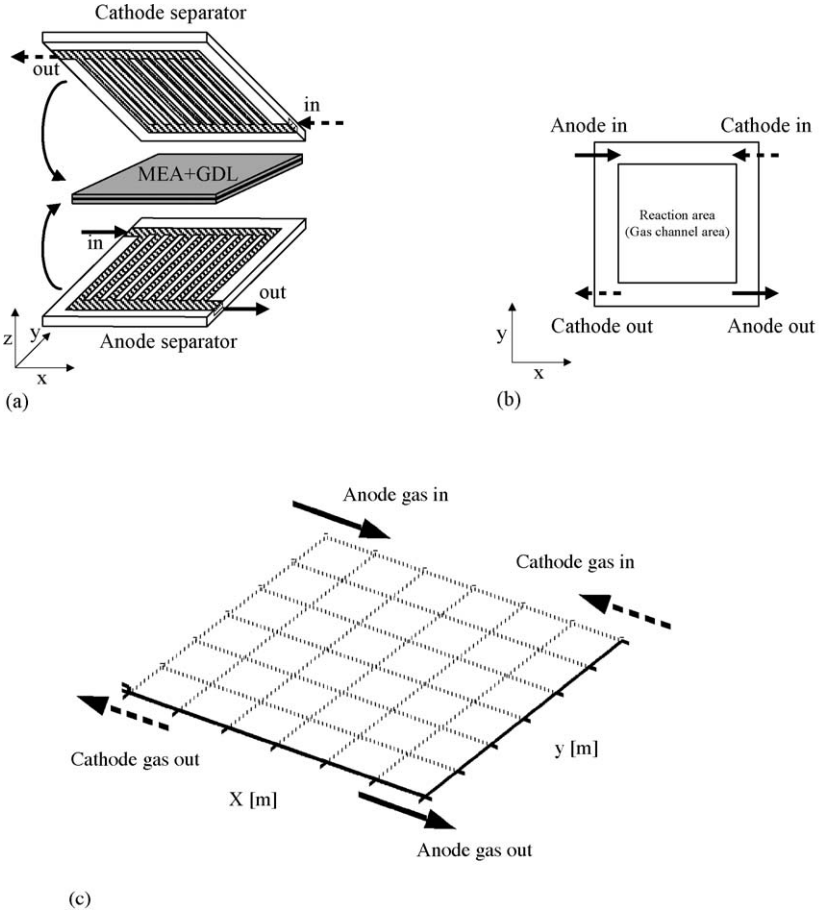

Fig. 13. Developed view of single cell and gas flow pattern with separators A–D. (a) Developed view of single cell (the anode separator and the cathode separator are the same); (b) gas flow pattern (viewpoint: from back of the cathode separator); (c) gas flow pattern (viewpoint: in Figs. 15 and 16).

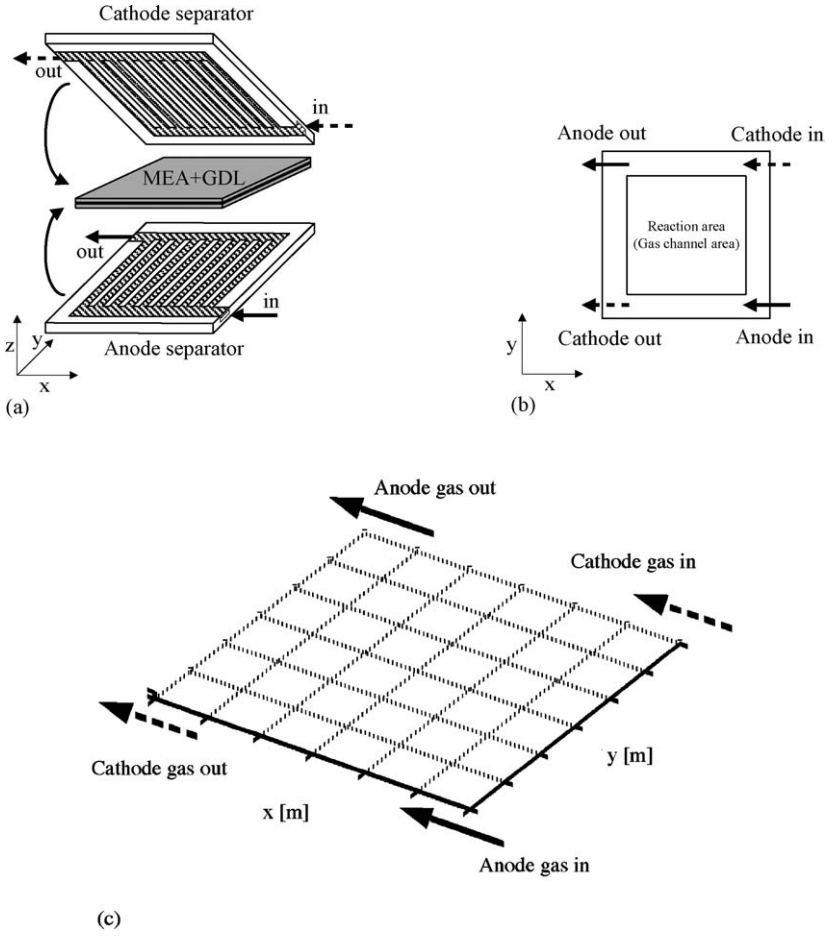

Fig. 14. Developed view of single cell and gas flow pattern with separator E. (a) Developed view of single cell (the anode separator and the cathode separator are different); (b) gas flow pattern (viewpoint: from back of the cathode separator); (c) gas flow pattern (viewpoint: in Figs. 15 and 16).

designed to unify the pressure drop in each channel by means of controlling the pressure gradient in inlet and outlet header section with curved walls. In case of parallel separator, gas flow rate of cathode side is larger than that of anode side, and it is thought that the cathode gas flow rate in distant channel from inlet is larger than that in near channel from inlet. Therefore, the different shape separator between anode side and cathode side were used on the basis of such condition. Fig. 13 shows the developed view of single cell and gas flow pattern with separators A–D. In case of separators A–D, both anode and cathode side separators were the same. As the same separators were put together like Fig. 13(a), gas flow patterns are shown in Fig. 13(b). And these gas flow pattern from the same point of view in Figs. 15 and 16 that are current density distribution and solid phase distribution, respectively, are shown in Fig. 13(c). Accordingly, in case of separator A, the gas flow pattern was parallel between anode gas and cathode gas in reaction area. And Yi and Nguyen [6] showed that current density and temperature distributions in case of coflow were more uniform than those in case of counterflow. Fig. 14 shows the developed view of single cell and gas flow pattern with separator E. In case of separator E, both anode and cathode side separators were different from each other, and the inlet and the outlet of anode gas were different from those of separators A–D. As the anode and cathode separators were put together like Fig. 14(a), gas flow patterns are shown in Fig. 14(b). As a result, the gas flow pattern of separator E was counter between anode gas and cathode gas in the reaction area. And this gas flow pattern from the same point of the view in Figs. 15 and 16 are shown in Fig. 14(c). Table 5 shows the dimensions of MEA, GDL and separator, and Table 6 shows calculation condition. It was supposed that physical properties were constant, because the effect of changing gas composition in cell on physical properties was little.

Fig. 15 shows the calculation result of current density distribution in each separator. In this figure, the current density with separator A was high at the upper side of the channel and low at the lower side of the channel. Because oxygen concentration were high at the upper side of the channel but they became low along the channel. And current density of the center channel was the lowest, because the gas flow rate of the center channel was the lowest in case of separator A, and the effect of oxygen concentration overvoltage became large. The current density with separators B and C was high at the center of the cell, because this area was middle of both

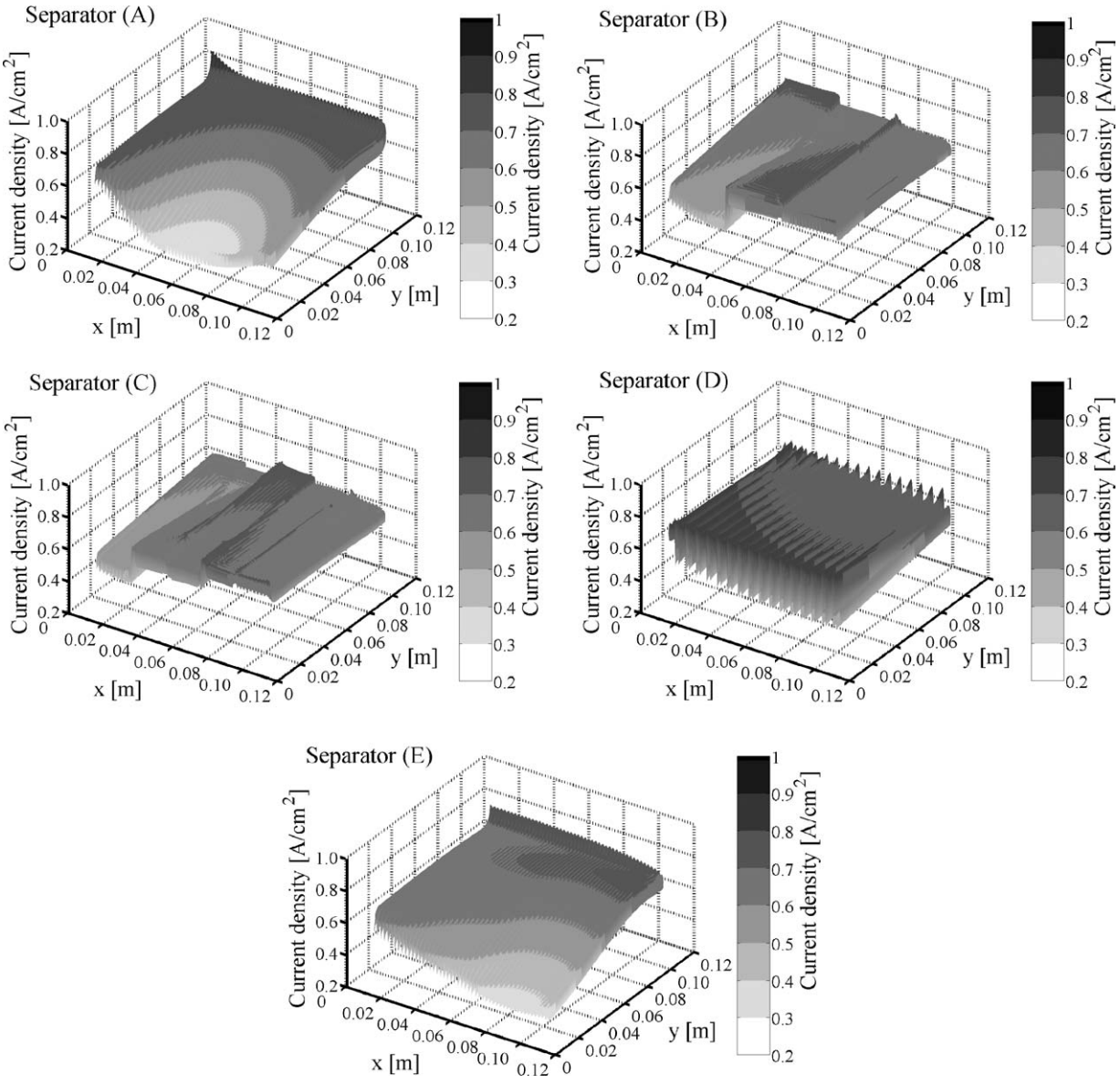

Fig. 15. Calculation results of current density distribution.

Table 5
Dimensions of MEA, GDL and separator of single cell in PEFC reaction and flow analysis

MEA	
Thickness of membrane (μm)	30
Size of catalyst layer (mm^2)	100 × 100
Amount of Pt ($g\,m^{-2}$)	3.0
GDL	
Size (mm^2)	100 × 100
Thickness (mm)	300
Separator	
Channel width (mm)	1
Shoulder width (mm)	1
Channel depth (mm)	1
Inlet and outlet width (mm)	5
Number of channel	A: 50, B: 16, C: 10, D: 16, E: 50
Distance from cooling plate (mm)	7

anode and cathode gas channel, and anode relative humidity and oxygen concentration were not very low. Therefore, the influence of the resistance and concentration overvoltage was little in the area. As each channels of separator D meander separately, the area of the high current density is close to that of the low current density, and that is distributed. The current density distribution with separator E was more uniform than that with separator A. However, that was not uniform perfectly, and the current density at the distant area from inlet was larger than that at the near area from inlet. From the above-mentioned, it followed that the current density distribution was different by the difference of the separator shape.

Fig. 16 shows solid phase temperature distribution of each separator. Compared with current density distribution of Fig. 15, solid phase temperature was high at the area

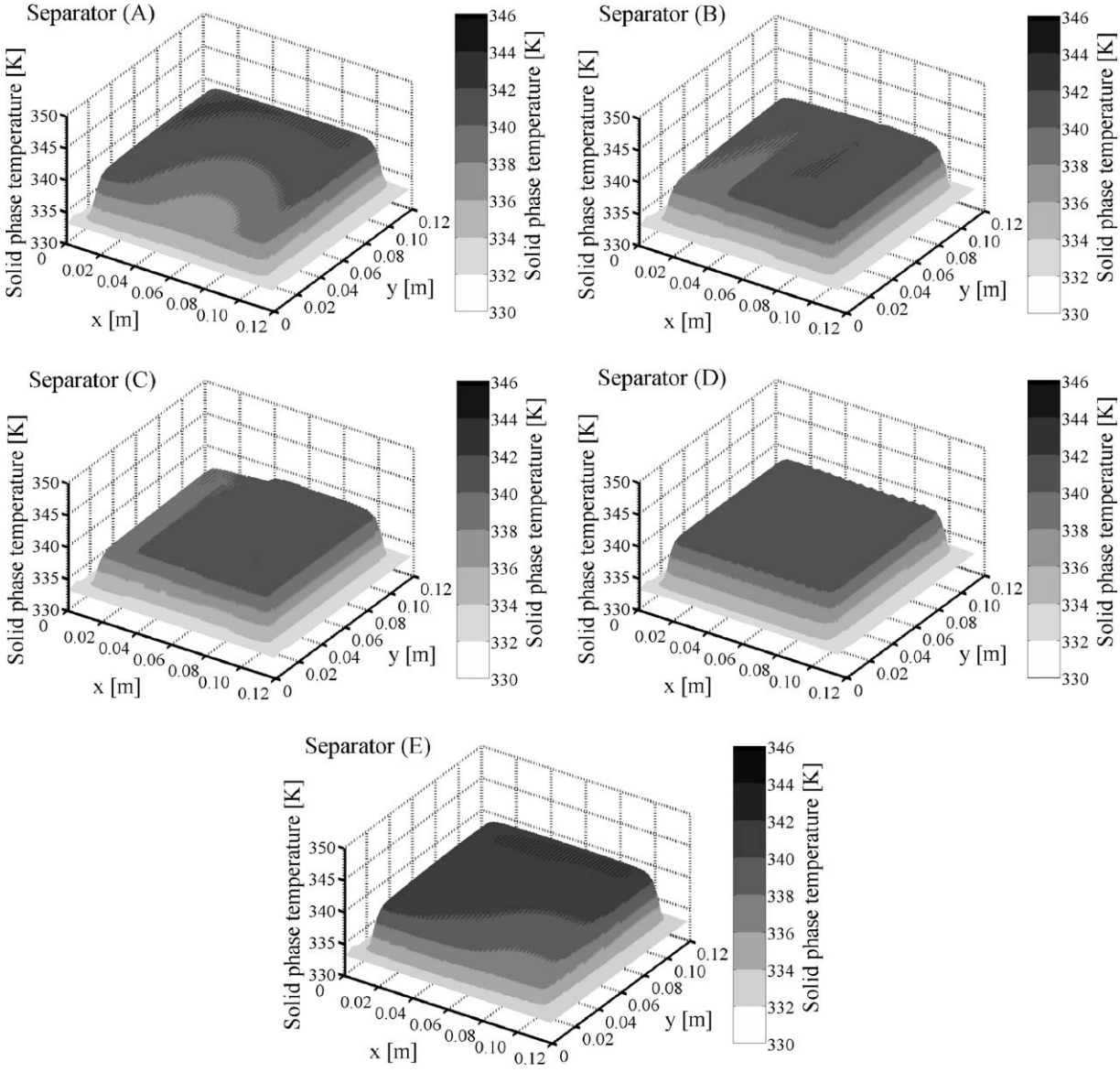

Fig. 16. Temperature distribution of solid phase.

of high current density because of the calorific value. In this study, cooling plates were inserted between every three cells, and the length of heat conduction between cooling plate and solid phase was lengthened three times as long as the thickness of single cell. It was expected that the temperature distribution of each cell was more complex by the heat conduction from the neighboring cell in actual stack, but the rough condition could be estimated by this analysis.

It was thought that the gas flow rate of cathode was not more uniform than that of anode because gas flow rate and inertial force are large. Fig. 17 shows the distribution of the cathode gas flow rate in each separator. As the channel number was different in each separator, the right edge of a horizontal axis is expressed to the channel near the inlet, the left edge of a horizontal axis is expressed to the channel near the outlet. The value of vertical axis is each groove flow rate divided by the average flow rate. In case the gas flow rate is uniform, this value of vertical axis is 1 all over the channel. In the separator A, the gas flow rate of the channel that was the nearest the outlet was 3.3 times as much as mean value, and the gas flow rate of the central channel was 0.6 times as much as mean value. So, the gas flow rate distribution of separator A was the largest in any separators, and the ununiformity of the gas flow rate generated the current density distribution of separator A. Because of improvement of header shape, the flow field in separator E is more uniform than in separator A. But the gas flow rate was not uniform perfectly even in separator E, and the gas flow rate of far side from the cathode inlet was the largest.

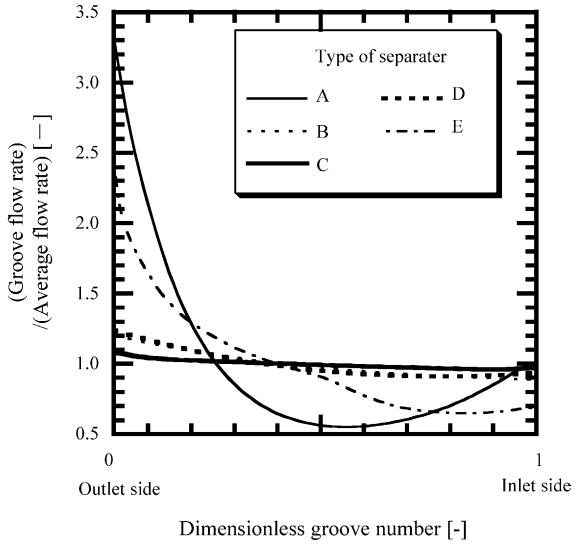

Fig. 17. Calculation result of gas flow rate distribution.

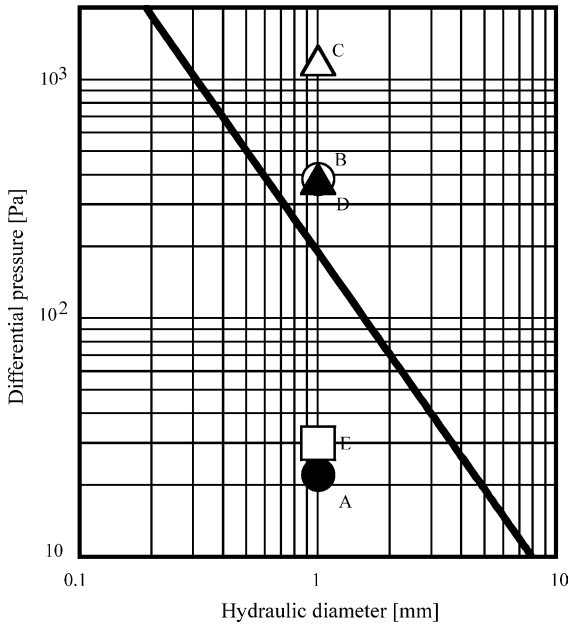

Fig. 18. Relationship between separator shape and ejection of water.

The gas flow rates of the other separator were distributed between 0.9 and 1.2 times as much as mean value, and were uniform comparatively, because the channel became longer by meandering the channel, and pressure drop of the channel became much larger than that of header. Accordingly, that of the separator C that has the longest channel was the most uniform.

The minimum pressure drop in the channel of each separator is shown in Fig. 18. The horizontal axis shows the width of the channel, and the vertical axis shows the differential pressure between the inlet and the outlet of the channel. The curve line in Eq. (35) obtained from the water ejection experiment. It was found that it was difficult to eject water in separators A and E because the pressure drop was below the ejection line, and that it was possible to eject it in other separators because the values were above the line. In addition, if the channel is bent to prevent water from blocking, the important thing is not to bend to excess but to obtain the differential pressure exceeding Eq. (35).

Table 6
Calculation conditions of PEFC reaction and flow analysis

Pressure (MPa)	0.1
Operation temperature (K)	333
Humidifier temperature (K)	333
Cooling plate temperature (K)	333
Operation voltage (V)	0.5
Inlet flow rate ($m^3\ s^{-1}$)	
Anode	1.25×10^{-5}
Cathode	5.15×10^{-5}
Inlet gas composition (%)	
Anode	H_2: 99.0
	N_2: 1.0
Cathode	O_2: 21.0
	N_2: 79.0

5.3. Comprehensive evaluation of the performance of five kinds of separator

Fig. 19 shows average current density (a), current density distribution (b), solid phase temperature distribution (c), gas flow rate distribution (d) and cathode pressure drop (e) of each separator. In Fig. 19(a), it was found that average current densities were mutually equal. In Fig. 19(b), the values of bar graph shows the difference between the maximum value and the minimum value of current density, and that of separator A was the largest, because the gas flow rate distribution was more marked than other separators. In Fig. 19(c), the values show the difference between the maximum value and the minimum value of the solid phase temperature, and that of separator D was the lowest. As the area of high current density was close to that of the low current density in separator D, the temperature difference was reduced by the heat conduction in the solid phase. On the other hand, that of separators A and E was the highest, because the heating value was different locally by ununiform gas flow distribution. In Fig. 19(d), it is a comparison of the values in which the maximum gas flow rate is divided by minimum gas flow rate on cathode, and that of separator A was the largest. In Fig. 19(e), the cathode pressure drop of separator C was the largest, and the reason for this was that the channel of separator C was longer than that of others.

As remarkable current density and temperature distribution have a bad influence on the safety, durability and driving efficiency of PEFC, it is necessary to make these distributions uniform as much as possible. And in order to make the cell output stable, it is important to be able to eject condensed water. Moreover, the pressure drop has to be as low as possible for the purpose of reduction of gas supply power. Consequently, separator D that satisfies these necessary con-

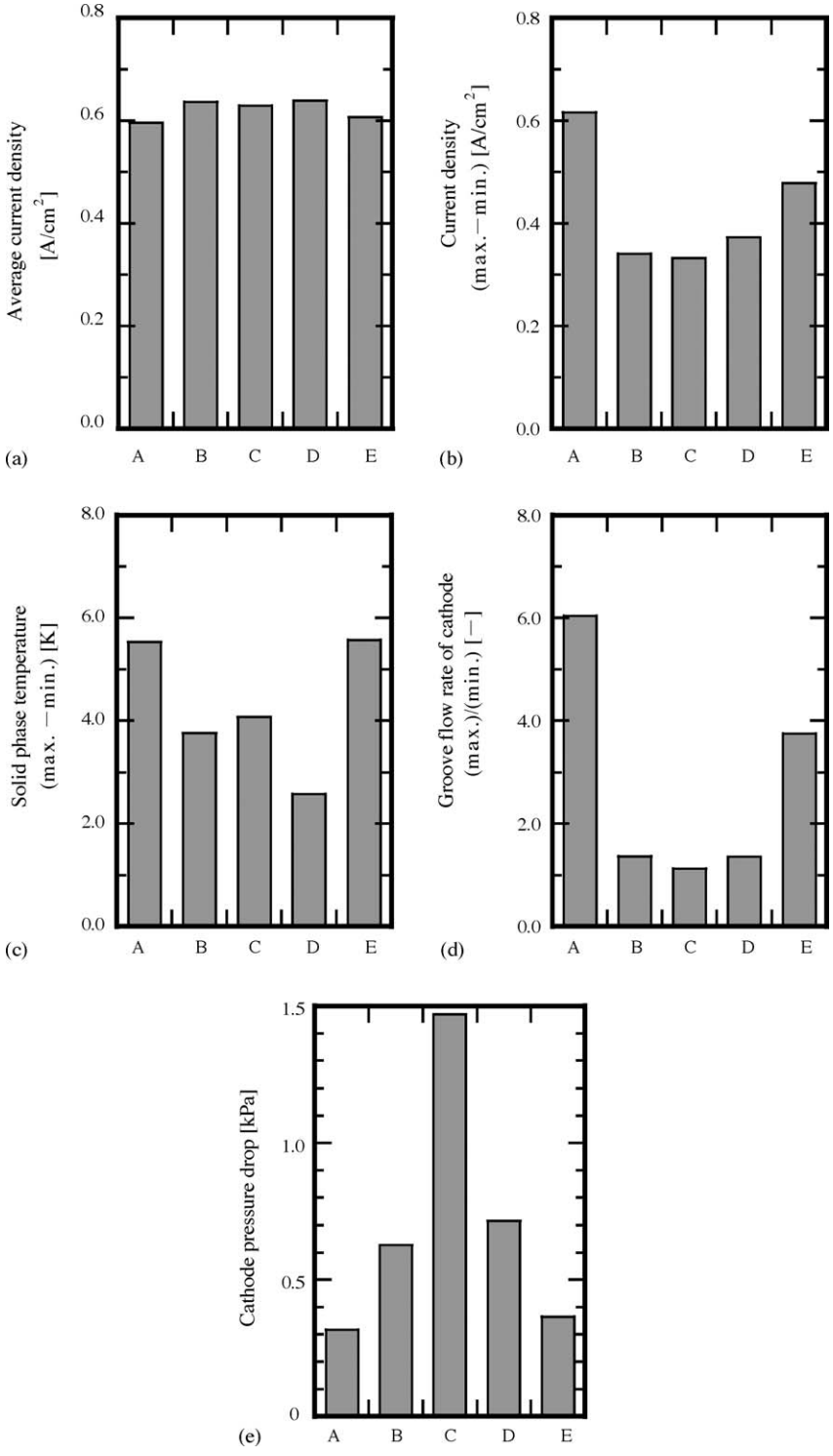

Fig. 19. (a–e) Comprehensive performance evaluation of five kinds of separators.

ditions was the best separator. However, the current density distribution changes by operating condition, such as cell temperature, humidification and gas flow rate, so it is necessary to examine it in a different condition. In addition, it is necessary to examine water ejection experiment in detail by changing the material and shape of channel.

6. Conclusion

In order to make the PEFC reaction model, the effects of cell temperature and oxygen and hydrogen concentration on the output characteristic of PEFC were examined experimentally, and the appropriateness of calculation results was

confirmed. Next, this PEFC reaction model was combined with thermal flow analysis model, and PEFC reaction and flow analysis model of actual size was made. Furthermore, five kinds of separators were evaluated with this model from the viewpoint of gas flow condition, current density distribution, cell temperature distribution, pressure drop and ejection performance of liquid water. And the water ejection differential pressure was investigated by experiment. The following results were obtained by these examinations:

1. Average current densities of each separator were almost same.
2. The current density distribution was caused by the concentration distribution resulted from ununiformity of gas flow rate.
3. In parallel channel separator, as gas flow rate distribution was remarkable, the distributions of concentration, current density and solid phase temperature became large, and it is difficult to eject liquid water. But those distributions were decreased by improvement of the shape of header.
4. In serpentine channel separator, gas flow rate, current density and temperature were more uniform than that of parallel separator. But, even if the channel is lengthened, it does not influence these distributions so much, and the pressure drop increases.
5. In semi-serpentine channel separator, the parts of high and low current density were dispersed and close to each other. And the solid phase temperature was unified.

The PEFC reaction model was developed for the purpose of simulating actual cell condition by fitting several parameters with experimental results. But this model has many assumptions. In our future study, it is expected that this model will be improved to apply in the various conditions.

References

[1] D.M. Bernardi, M.W. Verbrugge, Mathematical model of a gas diffusion electrode bonded to a polymer electrolyte, AIChE J. 37 (8) (1992) 1151–1163.
[2] D.M. Bernaldi, M.W. Verbrugge, A mathematical model of the solid-polymer-electrolyte fuel cell, J. Electrochem. Soc. 139 (9) (1992) 2477–2491.
[3] T.E. Springer, T.A. Zawodzinski, S. Gottesfeld, Polymer electrolyte fuel cell model, J. Electrochem. Soc. 138 (8) (1991) 2334–2342.
[4] T.F. Fuller, J. Newman, Water and thermal management in solid-polymer-electrolyte fuel cells, J. Electrochem. Soc. 140 (5) (1993) 1218–1225.
[5] T.V. Nguyen, R.E. White, A water and heat management model for proton-exchange-membrane fuel cells, J. Electrochem. Soc. 140 (8) (1993) 2178–2186.
[6] J.S. Yi, T.V. Nguyen, An along-the-channel model for proton exchange membrane fuel cells, J. Electrochem. Soc. 145 (4) (1998) 1149–1159.
[7] S. Um, C.Y. Wang, K.S. Chen, Computational fluid dynamics modeling of proton exchange membrane fuel cells, J. Electrochem. Soc. 147 (12) (2000) 4485–4493.
[8] Z.H. Wang, C.Y. Wang, K.S. Chen, Two-phase flow and transport in the air cathode of proton exchange membrane fuel cells, J. Power Sources 94 (2001) 40–50.
[9] S. Dutta, S. Shimpalee, J.W. Van Zee, Three-dimensional numerical simulation of straight channel PEM fuel cells, J. Appl. Electrochem. 30 (2000) 135–146.
[10] T. Berning, D. Lu, N. Djilali, Three-dimensional computational analysis of transport phenomena in a PEM fuel cell, J. Power Sources 106 (2002) 284–294.
[11] S. Mazumder, J.V. Cole, Rigorous 3-D mathematical modeling of PEM fuel cells model predictions with liquid water transport, J. Electrochem. 150 (11) (2003) 1510–1517.
[12] P.-W. Li, L. Schaefer, Q.-M. Wang, T. Zhang, M.K. Chyu, Multi-gas transportation and electrochemical performance of a polymer electrolyte fuel cell with complex flow channels, J. Power Sources 115 (2003) 90–100.
[13] S. Um, C.Y. Wang, Three-dimensional analysis of transport and electrochemical reactions in polymer electrolyte fuel cells, J. Power Sources 125 (2004) 40–51.
[14] A.A. Kulikovsky, Quasi three-dimensional modeling of the PEM fuel cell: comparison of the catalyst layers performance, Fuel Cells 1 (2001) 162–169.
[15] C. Marr, X. Li, Composition and performance modeling of catalyst layer in a proton exchange membrane fuel cell, J. Power Sources 77 (1999) 17–27.
[16] H. Yoshikawa, Y. Hishinuma, T. Chikahisa, Performance of a polymer electrolyte fuel cell for automotive applications, Trans. JSME 66 (2000) 3218–3225.
[17] A. Parthasarathy, S. Srinivasan, J. Appleby, Temperature dependence of the electrode kinetics of oxygen reduction at the platinum/Nafion interface a microelectrode investigation, J. Electrochem. Soc. 139 (1992) 2530–2537.